RSC Advances

PAPER

View Article Online
View Journal | View Issue

Cite this: *RSC Adv.*, 2025, **15**, 29013

Comparison of the properties of polyimides derived from various dianhydride and diamine monomers

Lee Ku Kwac,[ab] Byung-Joo Kim[c] and Jin-Hae Chang *[b]

Received 13th July 2025
Accepted 8th August 2025

DOI: 10.1039/d5ra05012j

rsc.li/rsc-advances

Dianhydrides 4,4′-(4,4′-isopropylidenediphenoxy)bis(phthalic anhydride) (BPADA) and dicyclo-hexyl-3,4,3′,4′-tetracarboxylic dianhydride (HBPDA) were reacted with four different diamines to synthesize eight polyimide (PI) films through various heat treatment processes. BPADA contains aromatic benzene, whereas HBPDA contains alicyclic cyclohexane. The four diamine monomers contained either a linear benzene, highly electronegative trifluoromethyl (–CF_3) group, bulky sulfone (–SO_2–) group, or methyl (–CH_3) group between the benzene rings. The PIs obtained using the four different diamines and BPADA dianhydride were designated as series (I), while the PIs synthesized using HBPDA dianhydride were designated as series (II). To improve the physical properties of the synthesized PI films, all diamine structures contained hydroxy (–OH) groups capable of forming hydrogen bonds. The thermomechanical properties, optical transparencies, and solubilities of eight PI films synthesized from various monomer structures were investigated. Structure–property relationships were established through comparative analysis and film properties is also explained, and the results are compared. Overall, series (I), which contained aromatic dianhydride monomers, exhibited better thermomechanical properties than series (II) films, which contained cycloaliphatic dianhydride monomers. However, the optical transparency and solubility of the series (II) PIs were superior to those of the series (I) PI films.

1. Introduction

Glass is the most commonly used transparent substrate material in displays. Owing to its favorable optical properties, such as excellent transparency, high refractive index, low dispersion, and low birefringence, glass has applications in various industrial fields. However, as the scope of applications broadens and information becomes more pervasive in modern society, there is a growing desire to share information irrespective of location and time.[1,2] To fulfill this desire, technological advancements are needed to meet the demands for ultralight, low-power consumption, and flexible displays that are as lightweight and flexible as paper, as well as for energy supply devices capable of providing power from anywhere, such as solar cells. Flexible and portable electronics have garnered significant attention in academic and industrial settings. Consequently, despite the numerous advantages of glass, it can no longer meet the requirements of these applications solely based on its properties.[3,4]

Plastic substrates have long received attention as the most suitable materials for flexible displays.[5,6] Compared with ultrathin glass (UTG),[7] they are more resistant to impact, allow for continuous roll-to-roll processing, and exhibit excellent flexibility, making them ideal substrates for flexible displays.[8] However, these plastic substrates often exhibit poor inherent mechanical and heat resistance near the glass transition temperature (T_g) and high oxygen and moisture permeabilities, limiting their use as display materials. Among these, polyimides (PIs) stands out because of its thermal properties, which can potentially replace glass owing to its heat resistance and low coefficient of thermal expansion. However, its applications are constrained by its characteristic yellow color, which adversely affects its optical properties.[9–11]

In eliminating the yellow color of PI and creating a highly colorless and transparent PI (CPI), the purity of the monomer, moisture content of the solvent, and control of the PI structure play significant roles, with many of these factors being influenced by the PI structure. The distinctive yellow color of PI is caused by charge transfer complexes (CTCs) within and between the molecules.[12–14] Methods for reducing CTC formation are: (1) the introduction of a linkage group between the phenyl rings of the main chain; or (2) the introduction of a bulky group into the side chain. Alternatively, there are methods for (3) lowering the symmetry of the main-chain structure or (4) introducing a cycloaliphatic group.[15,16] The aforementioned methods enhance CPI film performance by increasing molecular flexibility, expanding intermolecular distances, or reducing CTC formation.

[a]*Graduate School of Carbon Convergence Engineering, Jeonju University, Jeonju 55069, Korea*

[b]*Institute of Carbon Technology, Jeonju University, Jeonju 55069, Korea*

[c]*Department of Materials Science and Chemical Engineering, Jeonju University, Jeonju 55069, Korea. E-mail: jhchang@jj.ac.kr*

CPI can find wide applications in electronic devices such as display glasses. Moreover, owing to their easy synthesis and potential for mass production, they can be utilized for various purposes, including plasma display panels (PDPs), liquid crystal displays (LCDs), and solar panels, and are gaining attention as alternative energy sources.[17] Recently, flexible and transparent materials such as indium tin oxide (ITO), characterized by a conductive oxide layer, have been extensively used in display substrates and microelectronics.[18–20] However, owing to its rarity and high cost, indium is classified as a strategic material in international relations, leading to numerous challenges in cross-border trade. Additionally, its utilization faces constraints owing to its fragility and limited flexibility resulting from the high-temperature glass plate processing required to achieve high purity as a display material.[21,22] Therefore, CPIs have emerged as the most suitable alternatives to overcome the limitations of glass and can be widely employed as polymer materials for bendable, flexible, and wearable electronic devices.[23,24]

Hydrogen bonds that occur between polymer chains or within the chains can increase the stability and physical and chemical properties of the polymer structure.[25,26] This stabilization influences the three-dimensional (3-D) structure of the polymer, affecting its thermomechanical properties and the chemical resistance of PI through intermolecular hydrogen bonding. The hydroxyl (–OH) groups included in polymer chains affect the polymer's solubility, melting point, boiling point, and coefficient of thermal expansion (CTE) through hydrogen bonding. These changes are crucial for ensuring the stability of polymers in various environments and regulating their interactions with different solvents.[27]

In this study, eight different PI structures were synthesized using two dianhydride monomers with aromatic and cycloaliphatic structures and four diamines containing –OH groups. An aromatic dianhydride with a rigid structure was used to enhance the heat resistance and mechanical properties of the PI films. Conversely, to improve their optical properties, an cycloaliphatic dianhydride that mitigates the CTC effect was used. 4,4′-(4,4′-isopropylidene-diphenoxy) diphthalic anhydride (BPADA) served as the aromatic dianhydride, while dicyclohexyl-3,4,3′,4′-tetracarboxylic dianhydride (HBPDA) was used as the cycloaliphatic dianhydride. Additionally, various diamines with –OH groups were employed to enhance the properties and solubility based on hydrogen bonding between the PI chains. Diamine monomers containing –OH groups include 3,3′-dihydroxybenzidine (BZ), 2,2-bis(3-amino-4-hydroxyphenyl)hexa-fluoropropane (FDN), bis(3-amino-4-hydroxyphenyl)sulfone (APS), and 2,2-bis(3-amino-4-hydroxyphenyl)propane (AHP). The PIs obtained using the four different diamines and BPADA dianhydride were designated as series (I), while the PIs synthesized using HBPDA dianhydride were designated as series (II).

The purpose of this study is to measure the thermomechanical properties, optical transparency, and solubility of PI films synthesized using various heat-treatment processes. Additionally, this study aims to compare the physical properties of the PI films synthesized using aromatic and cycloaliphatic dianhydride monomers with different diamine monomer structures.

2. Experimental

2.1. Materials

All the reagents, including BPADA and HBPDA as dianhydride monomers and BZ, FDN, APS, and AHP as diamine monomers, were purchased from TCI (Tokyo, Japan). *N*,*N*′-Dimethylacetamide (DMAc), used as a solvent, was purchased from Aldrich (Yongin, Korea) and was employed after complete removal of moisture by adding a molecular sieve (4 Å).

2.2. Synthesis of poly(amic acid) (PAA) and PI films

Because the synthesis methods of PAA and PI using dianhydride and diamine are the same, the synthesis method using BPADA and BZ is explained as an example. First, to obtain PAA, BPADA (5.20 g; 1.0×10^{-2} mol) and BZ (2.16 g; 1.0×10^{-2} mol) were dissolved in DMAc (70 ml) in a three-necked flask and stirred vigorously at room temperature in a nitrogen atmosphere for 48 h. To remove the solvent, the obtained PAA solution was poured onto a clean glass plate and kept under vacuum for 2 h at 50 °C and 1 h at 80 °C.

For a complete imidization reaction, DMAc that had not been completely removed and water molecules generated during the imidization reaction were simultaneously removed by maintaining a vacuum at 110 °C for 30 min, 140 °C for 30 min, and 170 °C for 2 h. Subsequently, the final PI film was manufactured by heat treatment at 195 °C for 2 h, 220 °C for 2 h, and 235 °C for 4 h. The detailed heat-treatment process for the PI film is presented in Table 1. After complete heat treatment, the PI film was cooled by exposure to air, soaked in a 3 wt% aqueous solution of hydrofluoric acid (HF) for approximately 24 h, and then slowly removed from the glass plate. The PI synthesis method using the structures of the diamines and dianhydrides in each series is shown in Scheme 1. The inherent viscosities (IV) of the synthesized PI varied depending on the type of monomer, with those of series (I) PIs ranging from 0.87 to 1.31 dL g^{-1} and those of series (II) PIs ranging from 0.92 to 1.13 dL g^{-1} (see Table 2).

2.3. Characterization

Fourier transform infrared spectroscopy (FT-IR; PerkinElmer, L1600300, London, UK) and ^{13}C magic angle spinning nuclear magnetic resonance (^{13}C MAS-NMR; Bruker 400 MHz Advance II NMR, Bruker, Berlin, Germany) were employed to confirm the structure of the synthesized PI. The Larmor frequency for ^{13}C MAS was $(\omega_0/2\pi) = 100.61$ MHz, and the MAS rate for ^{13}C was measured at 12 kHz to minimize the number of radiated sidebands. The NMR peaks were referenced to a signal corresponding to tetramethylsilane (TMS).

To investigate the thermal properties of the PI film, differential scanning calorimetry (DSC; 2-00915, Delaware, USA) and thermogravimetric analysis (TGA; SDT 0650-0439, Delaware, USA) were performed, and the temperature was increased at a rate of 10 °C min^{-1} under a nitrogen stream. To measure CTE,

Table 1 Heat treatment conditions of PI films

Sample	Temperature (°C)/time (h)/pressure (torr)
PAA	50/2/1 → 80/1/1
CPI	110/0.5/1 → 140/0.5/1 → 170/2/1 → 195/2/1 → 220/2/1 → 235/4/1

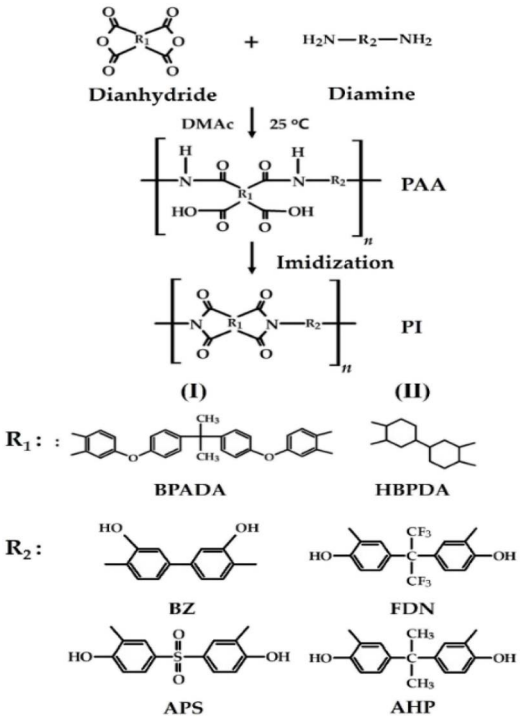

Scheme 1 Synthetic routes for PI films based on (I) BPADA and (II) HBPDA dianhydride monomers.

a thermomechanical analyzer (TMA; TMA SS6100, Tokyo, Japan) was used and heated at 5 °C min^{-1} with a load of 0.1 N. In this study, the values obtained during secondary heating in the 50–200 °C range were used. The structure of 3-D polymer chains was analyzed using the ChemDraw Office® computer program to investigate the correlation between physical properties and polymer chain structure.

Mechanical properties were measured using a universal tensile machine (UTM; Shimadzu JP/AG-50 KNX, Tokyo, Japan). The sample size in film form was 5 mm × 70 mm, and the crosshead speed was 5 mm min^{-1}. For each sample, the measurements were performed at least 15 times, and values outside the error range were excluded. The remaining values were then averaged. The measurement errors of ultimate tensile strength and initial modulus were within ±1 MPa and ±0.05 GPa, respectively.

To investigate optical transparency, the cut-off wavelength (λ_o) was determined using an ultraviolet-visible (UV-vis) spectrometer (Shimadzu UV-3600, Tokyo, Japan), and light transmittance (%) was measured at specific wavelengths. A spectrophotometer (Konica Minolta CM-3600, Tokyo, Japan) was used to measure the yellow index (YI). Additionally, to eliminate errors and obtain reliable results, the thickness of all measured film samples was kept constant within the range of 37 to 41 μm.

3. Results and discussion

3.1. FT-IR and ^{13}C-NMR analysis

FT-IR and ^{13}C-NMR experiments were conducted to determine the structures and synthesis states of the PI films, and the results are shown in Fig. 1 and 2, respectively.

Because of the broad peak observed in the range of 3563–3353 cm^{-1} for series (I), as shown in Fig. 1, the –OH group was identified in all the PIs prepared using the four diamines. The peaks at 1784–1778 cm^{-1} and 1709–1704 cm^{-1} confirmed the presence of the C=O carbonyl group. Additionally, the C–N–C peak, which is indicative of a successful imidization reaction, was observed at 1378–1369 cm^{-1}, confirming that imidization was complete. In the case of series (II), which was synthesized using HBPDA dianhydride, the peaks of each functional group were observed at similar positions. The –OH peak appeared as a gentle peak at 3408–3293 cm^{-1}, and the C=O peaks appeared at 1786–1763 cm^{-1} and 1712–1689 cm^{-1}. Furthermore, a C–N–C peak confirming the imide reaction was observed at 1394–1375 cm^{-1}.[28]

Unlike FT-IR, which uses the presence of functional groups to confirm the structure, ^{13}C-NMR can confirm the structure through accurate information on each carbon present in the polymer structure and thus complement the FT-IR results. The ^{13}C chemical shifts of the PIs synthesized using BZ diamine, BPADA, and HBPDA dianhydrides are shown in Fig. 2. In the

Table 2 Thermal properties of PI films

	(I) BPADA					(II) HBPDA				
Diamine	IV[a] (dL g^{-1})	T_g (°C)	T_D^{i}[b] (°C)	wt_R^{600c} (%)	CTE[d] (ppm per °C)	IV (dL g^{-1})	T_g (°C)	T_D^{i} (°C)	wt_R^{600} (%)	CTE (ppm per °C)
BZ	1.31	250	358	61	42	0.98	243	323	47	44
FDN	1.04	245	377	67	51	1.00	226	364	66	58
APS	1.11	227	342	59	43	0.92	217	299	44	46
AHP	0.87	218	336	40	47	1.13	203	274	23	50

[a] Inherent viscosity was measured at 27 °C by using a concentration of 0.1 dL g^{-1} solution in a *N*,*N*′-dimethyl acetamide. [b] Initial decomposition temperature at 2% weight loss. [c] Weight residue at 600 °C. [d] Coefficient of thermal expansion for 2nd heating is 50–200 °C.

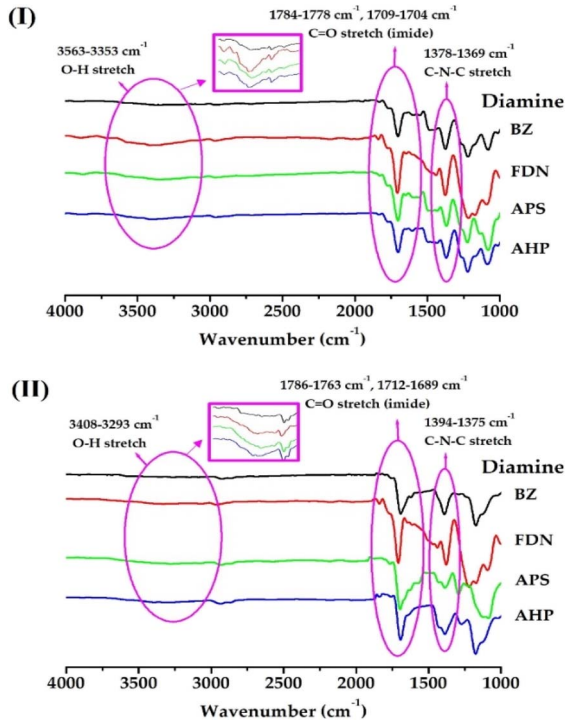

Fig. 1 FT-IR spectra of PIs based on (I) BPADA and (II) HBPDA dianhydride monomers.

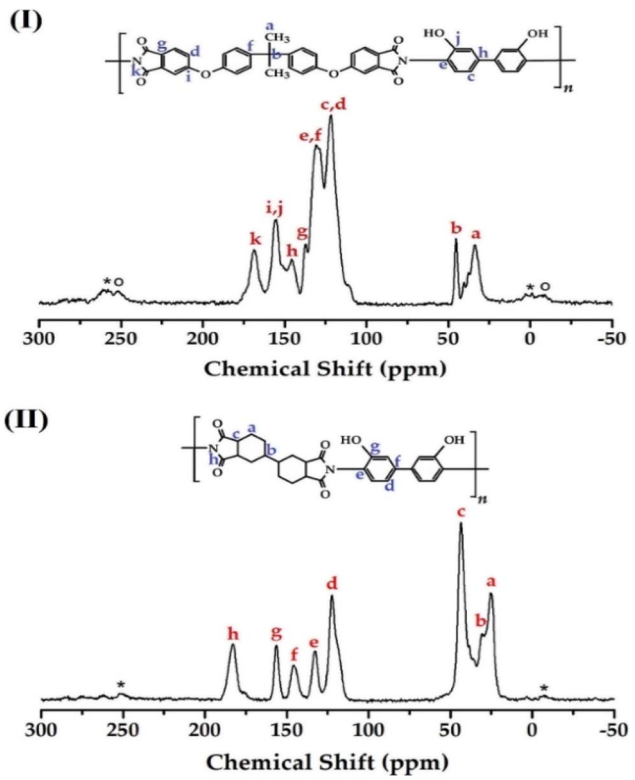

Fig. 2 ^{13}C-NMR chemical shifts of PI films: (I) BPADA/BZ and (II) HBPDA/BZ.

BPADA/BZ PI spectrum (Fig. 2(I)), chemical shifts for methyl (–CH_3, a) and isopropyl carbon (–C-$(CH_3)_2$, b) were observed at 33.81 ppm and 45.20 ppm, respectively. The chemical shifts corresponding to the phenyl carbon (c–j) peaks were observed at 121.87, 130.36, 137.14, 145.84, and 155.52 ppm, respectively. The carbonyl carbon (C=O, k) of the imide group was observed at 168.82 ppm. The rotating sidebands marked with asterisks (*) are the sidebands for peaks e and f, and those marked with (o) are the sidebands for peaks c and d.

Fig. 2(II) presents the chemical shifts of HBPDA/BZ. The chemical shifts of the carbon peaks (a–c) of the alicyclic structure were observed at 25.37, 30.44, and 43.49 ppm, respectively, and the chemical shifts of the carbon peaks (d–g) of the phenyl group were observed at 122.60, 133.00, 145.58, and 156.24 ppm, respectively. A peak corresponding to the imide carbon (h) was observed at 183.11 ppm. The small peak marked with an asterisk (*) is the rotating sideband of peak d from the phenyl carbon.[29] All the identified chemical shifts of carbon were consistent with the synthesized chemical structures. The NMR spectra of the FDN diamines are shown in SI Fig. S1 and S2, and the detailed chemical shifts of each peak are summarized in SI Tables S1 and S2.

3.2. Thermal property

Because the PI film is an amorphous polymer, its melting transition temperature (T_m) could not be determined using DSC. The thermal properties of the PI film can be explained primarily by its T_g. Generally, T_g is affected by segmental motion caused by changes in the rigidity and free volume of the polymer chain structure. Additionally, T_g can vary significantly depending on several factors, such as the structure of the monomer, type of substituents, hydrogen bonds present in the polymer chain, and chain mobility.[30,31] In this study, we attempted to

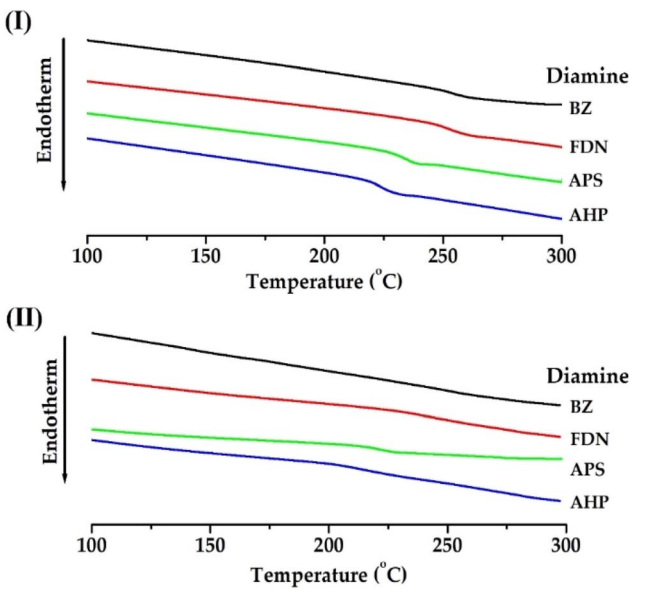

Fig. 3 DSC thermograms of PI films based on (I) BPADA and (II) HBPDA dianhydride monomers.

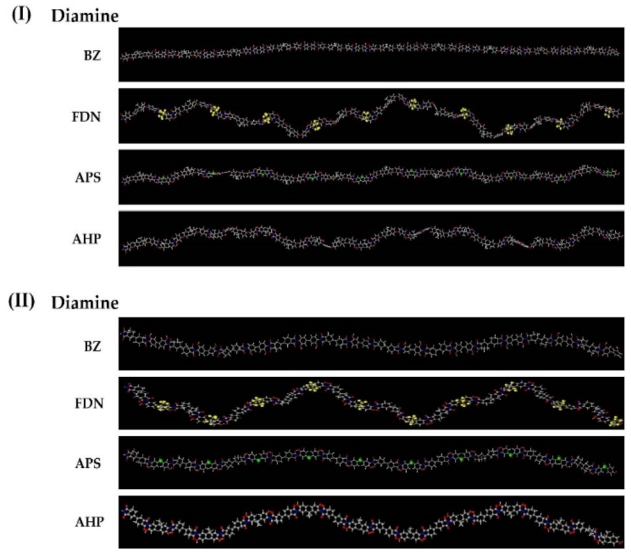

Fig. 4 Comparison of three-dimensional chemical structures of PI films based on (I) BPADA and (II) HBPDA dianhydride monomers.

determine how the structure of the PI film affects T_g using dianhydride and diamine monomers with different structures.

Table 2 presents the thermal characteristics measured using DSC, and the graphical data are shown in Fig. 3. The T_g values of PI using BPADA (series (I)) dianhydrides ranged between 218 and 250 °C, and those of HBPDA (series (II)) dianhydrides ranged between 203 and 243 °C. The 3-D polymer structures are shown in Fig. 4 to illustrate the correlation between the physical properties and the structure of the synthesized PI film.

In series (I), which uses BPADA anhydride, the BZ monomer structure consists of a benzene ring with no substituents other than –OH groups in the main chain and exhibited the highest T_g value (250 °C) due to the strong attraction between molecules resulting from the linear structure (see Fig. 4(I)). PIs derived from FDN exhibited a relatively high T_g value (245 °C) because the trifluoropropylene (–CF_3) structure, which has a large free volume, hinders the movement of chain segments and increases the heat energy required for movement.[32,33] However, this value is lower than that of the BZ structure, which has a rigid structure. APS also has a bulky sulfone (–SO_2–) substituent but showed a relatively low T_g value (227 °C) compared to the –CF_3-substituted FDN structure. However, AHP showed the lowest T_g value (218 °C) due to the chain's flexibility as well as the relative freedom of chain movement due to the methyl group (–CH_3). In series (II), which uses an alicyclic dianhydride, the T_g value according to the diamine structure showed the same tendency as in series (I), and the overall T_g value of the aromatic anhydride (I) was higher than that of the alicyclic anhydride (II). This is because it is more difficult for the main chain of BPADA, whose dianhydride is composed of an aromatic moiety, to undergo segmental motion by heating than that of HBPDA, which contains a cycloaliphatic moiety.[34,35]

To confirm the thermal stability of the PI film, TGA was employed to determine the initial decomposition temperature (T_D^i), which represents the temperature at which the initial 2 wt% loss occurred, and the residual weight at 600 °C (wt_R^{600}). The thermal stability results for PI according to the monomer structure are summarized in Table 2. BZ, which uses BPADA as the dianhydride (series (I)), is composed only of *p*-substituted benzene; therefore, its entire chain structure is linear. It showed a high T_D^i value of 358 °C due to its high thermal stability. Although FDN has a bent structure compared to the BZ structure (Fig. 4), it showed the highest T_D^i value (377 °C) due to the –CF_3 substituent, which has high thermal stability. In contrast, APS exhibited a very low T_D^i value of 342 °C. Generally, PIs containing –SO_2– groups exhibit low T_D^i values because the –SO_2– group can easily decompose into radicals owing to the conformational energy and steric hindrance within the chain at high temperatures.[36] AHP, which contains a propylene group as a substituent, showed the lowest T_D^i of 336 °C due to the alkyl group, which has very low thermal stability. As previously explained, the wt_R^{600} value was the highest (67%) for the PI containing FDN, which has high thermal stability, and the lowest for the PI containing AHP, which has the lowest thermal stability (40%).

The thermal stability of series (II), which was prepared using HBPDA dianhydride, was similar to that of series (I), which was synthesized using BPADA. For example, the PI synthesized using the FDN monomer exhibited the highest thermal stability, whereas the PI synthesized using AHP exhibited the lowest thermal stability. Overall, series (I) was thermally more stable than series (II). This is because, as already explained for

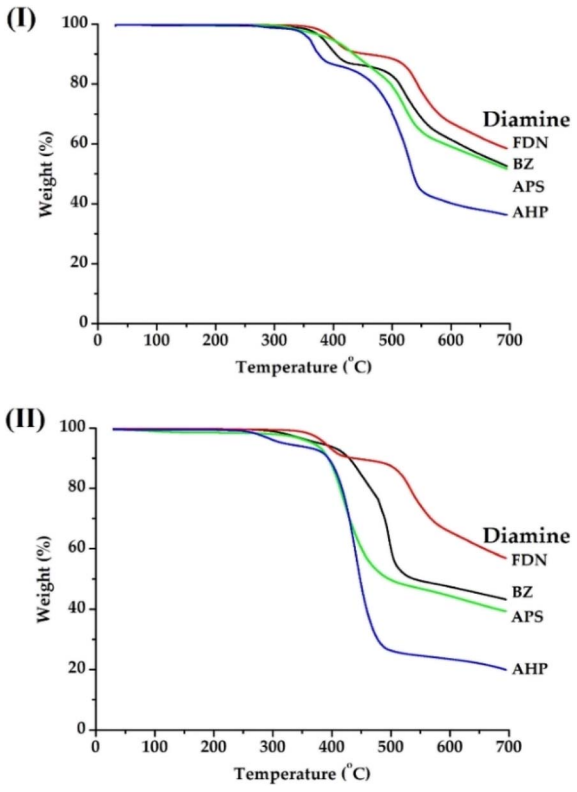

Fig. 5 TGA thermograms of PI films based on (I) BPADA and (II) HBPDA dianhydride monomers.

T_g, the aromatic structure that makes up PI has higher thermal stability than cycloaliphatic structures.

Two stages of thermal decomposition were observed upon heating all the PI films, as shown in the TGA thermogram in Fig. 5. This phenomenon occurs because PI containing the –OH group changes to polybenzoxazole (PBO) through thermal rearrangement (TR) at high temperatures.[37,38] For series (I) and series (II), PI is completely converted to PBO through the TR process at temperatures in the ranges of approximately 400–550 °C and 350–550 °C, respectively. Series (II), which has a cycloaliphatic structure with low thermal stability, exhibited a lower TR temperature range than series (I), which has high thermal stability. Scheme 2 shows the reaction process in which a PI containing an –OH group transforms to PBO through the TR process.

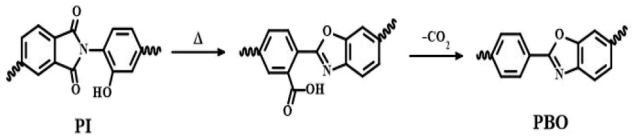

Scheme 2 Thermal rearrangement of polybenzoxazole from PI by heat treatment.

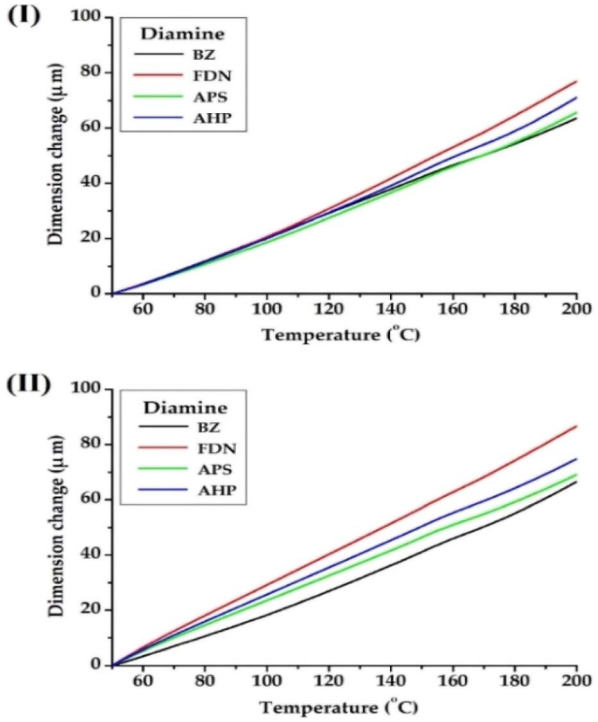

Fig. 6 TMA thermograms of PI films based on (I) BPADA and (II) HBPDA dianhydride monomers.

When polymers are heated, they generally expand along directions dictated by chain mobility, often more significantly perpendicular to the backbone direction. Therefore, if a polymer has an aromatic structure with high thermal stability or a rigid chain orientation of a linear structure, it interferes with heat transfer and slows thermal expansion. The results of using TMA to investigate the CTE of the polymer films are summarized in Table 2.

The CTE value depends on the overall chain structure of the polymer.[39–41] As shown in Fig. 4, the PI using the BZ monomer was the best because it had the straightest structure. In contrast, FDN, which has a bent structure containing large substituents in the main chain, showed the worst value. For example, in series (I), BZ showed the lowest CTE value at 42 ppm per °C, but FDN showed the highest CTE value at 51 ppm per °C. Additionally, the APS and AHP showed median values depending on the overall structure of their chains (see Table 1). This tendency also appeared in series (II), and as explained previously for T_g and T_D^i, the CTE value of series (I) was superior to that of series (II). The TMA thermograms for each series, according to the various monomer structures, are shown in Fig. 6.

3.3. Mechanical properties

A UTM was conducted to determine the strength and durability of that the PI film could withstand per unit area were measured, along with the elongation at break (EB). The results are summarized in Table 3. Series (I), which has a BZ structure (the 3-D structure is shown in Fig. 4), exhibited the highest final tensile strength and initial modulus because of its rigid rod-shaped main chain structure, which does not contain any substituents.[42,43] This linear chain structure is expected to have additional physical properties that can be enhanced through intermolecular hydrogen bonding using the –OH group of the chain. However, because FDN contains large substituents and has a bent overall structure, its mechanical properties are significantly inferior to those of BZ. In this bent-chain structure, the enhancement of the physical properties due to the extra

Table 3 Mechanical properties of PI hybrid films

	(I) BPADA			(II) HBPDA		
Diamine	Ult. str.[a] (MPa)	Ini. mod.[b] (GPa)	EB[c] (%)	Ult. str. (MPa)	Ini. mod. (GPa)	EB (%)
BZ	114	3.17	7	84	2.47	6
FDN	81	2.42	4	48	2.36	4
APS	106	2.52	6	73	2.41	6
AHP	91	2.26	5	55	1.74	3

[a] Ultimate strength. [b] Initial modulus. [c] Elongation at break.

Table 4 Optical properties of PI films

	(I) BPADA				(II) HBPDA			
Diamine	Thickness[a] (μm)	λ_o[b] (nm)	500 nm^{trans} (%)	YI[c]	Thickness (μm)	λ_o (nm)	500 nm^{trans} (%)	YI
BZ	40	397	61	38	41	351	79	18
FDN	39	380	87	3	38	331	90	1
APS	38	389	81	20	37	339	83	10
AHP	41	383	83	10	39	334	86	2

[a] Film thickness. [b] Cut-off wavelength. [c] Yellow index.

hydrogen bonding, which can occur in a straight structure, cannot be expected. The APS monomer has a nearly linear overall 3-D polymer chain shape (see Fig. 4) and better mechanical each PI film under tension. The ultimate strength and initial modulus properties than the FDN monomer because of the highly electronegative –SO_2– functional group. The mechanical properties of the AHP monomer are the worst because it contains a flexible alkyl group as a substituent.[44]

For example, series (I), which has a BZ monomer structure, showed the highest final strength and initial modulus of 114 MPa and 3.17 GPa, respectively, because the entire polymer chain was composed of a linear structure. However, the PI derived from FDN showed low ultimate strength and initial modulus (81 MPa and 2.42 GPa, respectively) owing to the bent structure of the polymer main chain (Fig. 4). This explanation can also be applied to series (II), which consists of cycloaliphatic monomers. For the reasons already explained above, the ultimate strength and initial modulus values of the PI containing the BZ monomer were the highest (84 MPa and 2.47 GPa), and the inclusion of the FDN monomer resulted in significantly lower values of both the ultimate strength and initial modulus (48 MPa and 2.36 GPa, respectively). When AHP was used in any of the series, the initial modulus value was the lowest (2.26 GPa (series (I)) and 1.74 GPa (series (II))). The reason for such low values is the presence of monomers containing flexible alkyl groups and the overall bent structure of AHP, as shown in Fig. 4. The EB values were usually 4–7% for series (I) and 3–6% for series (II), depending on the amine monomer structure; however, there was no significant difference between them.

Between the two series, series (I) exhibited better mechanical properties than series (II). These results were attributed to the structural differences between the two series due to the presence of linear and rigid aromatic dianhydride monomers in series (I) and flexible cycloaliphatic monomers in series (II).

3.4. Optical transparency

Typically, PI films appear dark brown because the π electrons in the PI main chain absorb violet and cyan colors in the visible range and reflect yellow and red colors between the wavelengths of 400 and 500 nm.[45] To determine the optical transparency of the PI film according to the different monomers, the λ_o and transmittance at 500 nm (500 nm^{trans}) were measured. The YI was also measured to assess the color of the film. The YI can be obtained using the following formula (ASTM E313-96, DIN 6167): $YI = 100 \times (aX - bZ)/Y$, where a and b represent the red and yellow values, respectively, and X, Y, and Z represent the tristimulus values.[46]

The results for the optical transparency of the PI film, as determined using UV-vis spectroscopy, are shown in Table 4 and Fig. 7. The λ_o values of all PI films were below 400 nm, indicating that radiation absorption began in the near-UV range before the visible spectrum. Regardless of the type of dianhydride, the λ_o and YI values of PIs using BZ diamine were the highest, and the values of 500 nm^{trans} were the lowest. Additionally, the λ_o and YI values of the PI using FDN diamine were

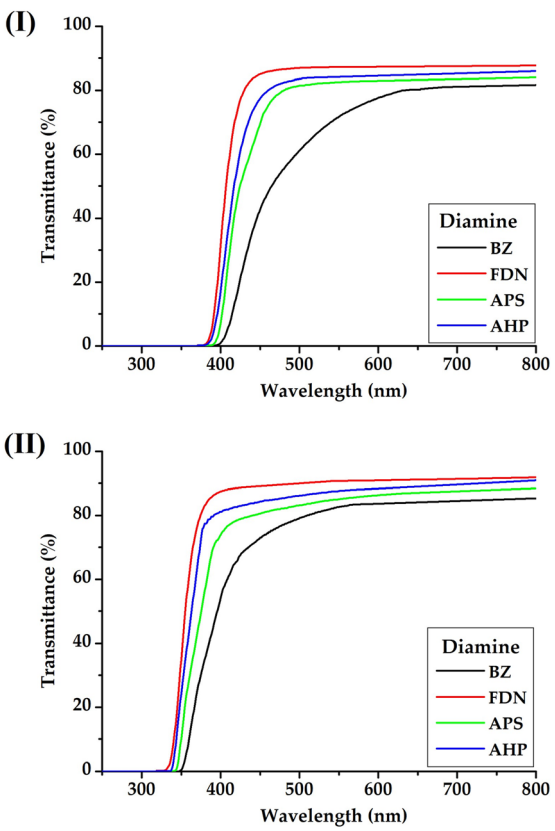

Fig. 7 UV-vis transmittances of PI films based on (I) BPADA and (II) HBPDA dianhydride monomers.

Fig. 8 Photographs of PI films based on (I) BPADA and (II) HBPDA dianhydride monomers.

the lowest, and the value of 500 nm^{trans} was the highest. These results are directly related to the formation of the CTC and the main-chain structure of the polymer. For example, for series (I), the highest λ_o and YI values of the PI with BZ were 397 nm and 38, respectively, whereas for the PI with FDN, the lowest values of 380 nm and 3 were observed. The difference in these values is because the PI using BZ has a rod-shaped straight-chain structure, which enables the formation of CTCs between chains and therefore exhibits lower optical properties.

In contrast, FDN monomers not only have large substituents but also strong electron-withdrawing groups (–CF_3) that prevent the formation of a CTC between the main chains and thus exhibit excellent optical properties.[47,48] The 500 nm^{trans} values can also be explained using the overall 3-D polymer chain structure described previously (see Fig. 4). Because the entire polymer chain of BPADA/BZ has a rigid rod-shaped structure, the 500 nm^{trans} value is greatly reduced owing to the CT complex generated between the main chains (61%). Conversely, BPADA/FDN PI has the highest 500 nm^{trans} value (87%) because it contains a strong electron-withdrawing substituent (–CF_3) that prevents CTC formation.

Films based on various monomer structures were visually observed by overlaying them directly on top of the university logo, as shown in Fig. 8. As mentioned earlier, the FDN and AHP films were the most colorless and transparent in both series, regardless of the anhydride structure. In contrast, when BZ and APS were used as monomers, the films exhibited darker colors. These color changes are closely related to CTC formation between the polymer chains, which is influenced by the structure of the monomers present in the polymer chain. However, as shown in Fig. 8, the logo was clearly visible through each of the PI films. A comparison of the overall results according to the type of dianhydride shows that the optical transparency of series (II) with HBPDA was better than that of series (I) with BPADA.

This is because PIs using cycloaliphatic dianhydride do not allow CTC formation because of the absence of π electrons in aromatic benzene. In particular, the YI of PI films using FDN and AHP in the cycloaliphatic series (II) is approximately 1–2, which is similar to that of poly(methyl methacrylate) (PMMA) and shows the characteristics of PI that can be used as a substitute for glass. It can be used not only as an electronic material for flexible displays, which have been widely studied recently, but also as a material to replace existing LEDs, PDPs, and electronic circuit substrates.

3.5. Solubility test

PI is a super-engineered polymer with insoluble and infusible properties and is composed of benzene and strong imide bonds along most of the main chain.[49,50] Consequently, they exhibit excellent thermomechanical properties and chemical resistance. However, their outstanding properties pose significant processing challenges. To address these drawbacks, attempts have been made to enhance their processability by introducing a flexible and curved structure to the monomers constituting the PI. Therefore, the solubility of PI is closely influenced by its monomer structure.[51–53]

Table 5 summarizes the solubility of the two films in various solvents. Series (I), which utilized aromatic benzene as a monomer base, generally exhibited low solubility in common solvents such as alcohol and acetone. However, it demonstrated excellent solubility in specialized solvents, such as pyridine, DMSO, NMP, and DMAc.

According to 3-D modelling (Fig. 4), PIs derived from FDN and AHP exhibited more twisted or curved chain conformations, which contributed to their improved solubility compared to the more linear structures of BZ and APS-based polymers. This increased solubility can be attributed to the ease with which solvents penetrate the empty space created by

Table 5 Solvent tests of PI films[a]

Monomer		MeOH	EtOH	Act	$CHCl_3$	CH_2Cl_2	Tol	THF	Py	DMF	DMSO	NMP	DMAc
(I) BPADA	BZ	×	×	×	×	×	×	×	△	◎	◎	△	◎
	FDN	×	△	○	△	△	○	△	◎	◎	◎	◎	◎
	APS	×	△	×	△	×	×	×	◎	◎	◎	◎	◎
	AHP	×	△	○	△	△	○	△	◎	◎	◎	◎	◎
(II) HBPDA	BZ	×	×	×	○	×	×	△	◎	◎	◎	◎	◎
	FDN	△	△	○	○	△	○	○	◎	◎	◎	◎	◎
	APS	×	△	△	○	△	×	△	◎	◎	◎	◎	◎
	AHP	△	△	○	○	△	○	△	◎	◎	◎	◎	◎

[a] ◎: excellent, ○: good, △: poor, ×: very poor. Act: acetone, Tol: toluene, THF: tetrahydrofuran, Py: pyridine, DMF: *N*,*N*′-dimethylformamide, DMSO: dimethyl sulfoxide, NMP: *N*-methyl-2-pyrrolidone, DMAc: *N*,*N*′-dimethylacetamide.

the curved structure. In contrast, series (II), which employed a cycloaliphatic monomer as the base, exhibited superior solubility in all solvents compared to series (I). This improvement is attributed to the use of monomers with cycloaliphatic structures, which have excellent solubility, resulting in an overall polymer chain structure that is more curved than that of series (I).[54]

4. Conclusion

This study investigated the properties of PIs synthesized from two distinct series of monomers: aromatic and cycloaliphatic dianhydrides. The results were compared according to their molecular structures. In particular, four amine monomers containing –OH groups were employed to synthesize novel PIs capable of forming intermolecular hydrogen bonds. The mechanism of their conversion into PBO structures upon high-temperature thermal treatment was also elucidated. Furthermore, all PIs obtained from the various monomer structures demonstrated potential applicability as flexible electronic materials for display devices.

To achieve this goal, we synthesized various types of PI films with different monomer structures and measured their thermo-mechanical properties, optical transparencies, and solubilities. PI films with a rigid and linear aromatic structure (series I) exhibited excellent thermomechanical properties but had low solubility and a dark color. In contrast, films with a flexible and bent cycloaliphatic structure (series II) showed colorless and transparent optical properties along with excellent solubility. In particular, among the two series, the PIs synthesized using the diamines FDN (YI: 1 and 3) and AHP (YI: 2 and 10) exhibited excellent optical transparency, making them more suitable for use as electronic materials in flexible displays.

The PI films developed in this study are suitable for applications requiring both excellent thermodynamic properties and optical transparency, including film-type flexible substrates, automotive touch panels, solar panel substrates, and rollable or wearable materials.

Author contributions

J.-H. Chang designed the project and wrote the manuscript. L. K. Kwac and B.-J. Kim prepared the samples and participated in the data analysis. All authors have read and agreed to the published version of the manuscript.

Conflicts of interest

There are no conflicts to declare.

Data availability

The datasets used and/or analyzed during the current study available from the corresponding author on reasonable request.

Supplementary information is available. See DOI: **https://doi.org/10.1039/d5ra05012j**.

Acknowledgements

This research was supported by "Regional Innovation Strategy for Education (RISE)" through the National Research Foundation of Korea (NRF) funded by the Ministry of Education (MOE).

References

1 M. S. AL-Buriahi, N. S. Alsaiari, M. U. Baskin, I. O. Olarinoye and J. Rad, *Appl. Sci. Res.*, 2025, **18**, 101264.
2 Q.-F. Guan, Z.-C. Ling, Z.-M. Han, H.-B. Yang and S.-H. Yu, *Matter*, 2020, **3**, 1308–1317.
3 K.-I. Fukukawa and M. Ueda, *Polymer*, 2008, **40**, 281–296.
4 K.-J. Baeg and J. Lee, *Adv. Mater. Technol.*, 2020, **5**, 2000071.
5 N. Kant and P. Singh, *Mater. Today Proc.*, 2022, **43**, 2843–2849.
6 Y. Zhang, T. Zhang, Z. Huang and J. Yang, *Adv. Sci.*, 2022, **9**, 2105084.
7 M. H. Ha, J. K. Choi, B. M. Park and K. Y. Han, *J. Mech. Sci. Technol.*, 2021, **35**, 661–668.
8 J. Tan, F. Xie, J. Huang, C. Zhao, X. Liu, H. Liu, J. Yuan and Y. Liu, *React. Funct. Polym.*, 2023, **192**, 105703.
9 C. Huang, C. Zuo, X. Chen and W. Xing, *Adv. Membr.*, 2025, **5**, 100154.
10 D. Zhang, L. Li, Y. Wang, C. Zhang and C. Teng, *J. Sol. Gel Sci. Technol.*, 2023, **108**, 1–12.
11 H. J. Ni, J. G. Liu, Z. H. Wang and S. Y. Yang, *J. Ind. Eng. Chem.*, 2015, **28**, 16–27.
12 R. Sawada and S. Ando, *Macromolecules*, 2022, **55**, 6787–6800.
13 C. J. Bender, *Chem. Soc. Rev.*, 1986, **15**, 475–502.
14 X. Zhang, X. Li, L. Li and T. Shi, *J. Mol. Liq.*, 2024, **411**, 125691.
15 H. T. Zuo, F. Gan, J. Dong, P. Zhang, X. Zhao and Q. H. Zhang, *Chin. J. Polym. Sci.*, 2021, **39**, 455–464.
16 S. Yu, J. Zhou, A. Xu, J. Lao, H. Luo and S. Chen, *Chem. Eng. J.*, 2023, **469**, 143803.
17 Y. Xu, M. Zhang, Y. Pang, T. Zheng, L. Zhang, Z. Wang and J. Yan, *Eur. Polym. J.*, 2022, **179**, 111528.
18 J. Yoon, U. Kim, Y. Yoo, J. Byeon, S. K. Lee, J. S. Nam, K. Kim, Q. Zhang, E. I. Kauppinen, S. Maruyama, P. Lee and I. Jeon, *Adv. Sci.*, 2021, **8**, 2004092.
19 Y. Demirhan, H. Koseoglu, F. Turkoglu, Z. Uyanik, M. Ozdemir, G. Aygun and L. Ozyuzer, *Renewable Energy*, 2020, **146**, 1549–1559.
20 Y. Han, Z. Hu, W. Zha, X. Chen, L. Yin, J. Guo, Z. Li, Q. Luo, W. Su and C. Q. Ma, *Adv. Mater.*, 2022, **34**, 2110276.
21 Y. Lan, Y. Chen, J. He and J. Chang, *Vacuum*, 2014, **107**, 55–61.
22 X. Jiang, K. Chen, C. Li, Y. Long, S. Liu, Z. Chi, J. Xu and Y. Zhang, *ACS Appl. Mater. Interfaces*, 2023, **15**, 41793–41805.
23 Y.-Y. Liu, Y.-K. Wang and D.-Y. Wu, *J. Appl. Polym. Sci.*, 2022, **139**, e52604.
24 X. Li, M. Wang, N. Mushtaq, G. Chen, G. Li, X. Fang and A. Zhang, *Polymer*, 2023, **265**, 125579.

25 Y. Tian, L. Luo, Q. Yang, L. Zhang, M. Wang, D. Wu, X. Wang and X. Liu, *Polymer*, 2020, **188**, 122100.
26 Z. Yang, P. Ma, F. Li, H. Guo, C. Kang and L. Gao, *Eur. Polym. J.*, 2021, **148**, 110369.
27 G. Qian, H. Chen, G. Song, J. Yao, M. Hu and C. Chen, *J. Polym. Sci.*, 2020, **58**, 969–976.
28 D. L. Pavia, G. M. Lampman, G. S. Kriz and J. Vyvyan, *Introduction to Spectroscopy*, Cengage Learning, Boston, Massachusetts, USA, 2008, ch. 2, pp. 14–95.
29 D. L. Pavia, G. M. Lampman, G. S. Kriz and J. Vyvyan, *Introduction to Spectroscopy*, Cengage Learning, Boston, Massachusetts, USA, 2008, ch. 4, pp. 146–183.
30 Y. Na, S. Kang, L. K. Kwac, H. G. Kim and J.-H. Chang, *ACS Omega*, 2024, **9**, 12195–12203.
31 D. Li, D. Li, Z. Ke, Q. Gu, K. Xu, C. Chen, G. Qian and G. Liu, *J. Polym. Sci.*, 2023, **61**, 818–828.
32 S. Li, H. Zhu, F. Bao, X. Lan, H. Li, Y. Li, M. Ji, M. Wang, C. Zhu and J. Xu, *Polymer*, 2023, **283**, 126245.
33 Y. Wang, X. Liu, J. Shen, J. Zhao and G. Tu, *Polymers*, 2022, **14**, 4132.
34 X. Yan, F. Dai, Z. Ke, K. Yan, C. Chen, G. Qian and H. Li, *Eur. Polym. J.*, 2022, **164**, 110975.
35 H. Lei, B. Bao, W. Peng, L. Qiu, B. Zou and M. Huang, *Polym. Chem.*, 2022, **13**, 6606–6613.
36 Z. Wang, M. Zhang, E. Han, H. Niu and D. Wu, *Polymer*, 2020, **206**, 122884.
37 S. Luo, J. Liu, H. Lin, B. A. Kazanowska, M. D. Hunckler, R. K. Roeder and R. Guo, *J. Mater. Chem. A*, 2016, **4**, 17050–17062.
38 A. Yerzhankyzy, Y. Wang, F. Xu, X. Hu, B. Ghanem, X. Ma, M. Balcik, N. Wehbe, Y. Han and I. Pinnau, *J. Membr. Sci.*, 2023, **683**, 121764.
39 G. Song, X. Zhang, D. Wang, X. Zhao, H. Zhou, C. Chen and G. Dang, *Polymer*, 2014, **55**, 3242–3246.
40 Z. Yang, H. Guo, C. Kang and L. Gao, *Polym. Chem.*, 2021, **12**, 5364–5376.
41 L. Bai, L. Zhai, M. H. He, C. O. Wang, S. Mo and L. Fan, *Chin. J. Polym. Sci.*, 2020, **38**, 748–758.
42 J. Li, N. Yu, Y. Ding, T. Xu, G. Zhang, Z. Jing and X. Shi, *J. Cell. Plast.*, 2021, **57**, 717–731.
43 Z. Wu, J. He, H. Yang and S. Yang, *Polymers*, 2022, **14**, 1269.
44 M. Farkhondehnia and M. Maric, *React. Funct. Polym.*, 2023, **191**, 105683.
45 M. S. H. Akash and K. Rehman, *Essent. Pharm. Anal.*, 2020, 29–56.
46 C.-P. Yang and Y.-Y. Su, *Polymer*, 2005, **46**, 5778–5788.
47 T. Zhang, Y. Pan, C. Song, B. Huang and Z. Z. Huang, *Polym. Bull.*, 2020, **77**, 4077–4094.
48 B. Y. Zou, L. H. Qiu, H. Y. Lei, J. M. Liu, W. F. Peng, H. Q. Zhao, F. Bao and M. J. Huang, *Chin. J. Polym. Sci.*, 2023, **41**, 1599–1608.
49 S. R. Nagella and C. S. Han, *Nanomater*, 2023, **13**, 2090.
50 Y. Wu, S. Liu and J. Zhao, *ACS Omega*, 2022, **7**, 11939–11945.
51 H.-C. Yu, J.-W. Jung, J.-Y. Choi, S. Y. Oh and C.-M. Chung, *J. Macromol. Sci.*, 2017, **54**, 97–104.
52 A. Ghosh, S. K. Sen, S. Banerjee and B. Voit, *RSC Adv.*, 2012, **2**, 5900–5926.
53 H. Zheng, C. Wang, Z. Tao, C. Jiang, X. Zhao, J. Li and Q. Ren, *J. Electron. Mater.*, 2021, **50**, 6981–6990.
54 G. L. Jiang, D. Y. Wang, H. P. Du, X. Wu, Y. Zhang, Y. Y. Tan, W. Lin, J. G. Liu and X. M. Zhang, *Polymers*, 2020, **12**, 413.